Letter | Editors' Suggestion

Pressure-enhanced fractional Chern insulators along a magic line in moiré transition metal dichalcogenides

Nicolás Morales-Durán,[1,2,*] Jie Wang,[3,4] Gabriel R. Schleder,[5,6] Mattia Angeli,[5] Ziyan Zhu,[7] Efthimios Kaxiras,[4,5] Cécile Repellin,[8] and Jennifer Cano[9,2,†]

[1]*Department of Physics, The University of Texas at Austin, Austin, Texas 78712, USA*
[2]*Center for Computational Quantum Physics, Flatiron Institute, 162 5th Avenue, New York, New York 10010, USA*
[3]*Center for Mathematical Sciences and Applications, Harvard University, Cambridge, Massachusetts 02138, USA*
[4]*Department of Physics, Harvard University, Cambridge, Massachusetts 02138, USA*
[5]*John A. Paulson School of Engineering and Applied Sciences, Harvard University, Cambridge, Massachusetts 02138, USA*
[6]*Brazilian Nanotechnology National Laboratory (LNNano), CNPEM, 13083-970 Campinas, São Paulo, Brazil*
[7]*Stanford Institute for Materials and Energy Sciences, SLAC National Accelerator Laboratory, Menlo Park, California 94025, USA*
[8]*Université Grenoble Alpes, CNRS, LPMMC, 38000 Grenoble, France*
[9]*Department of Physics and Astronomy, Stony Brook University, Stony Brook, New York 11794, USA*

(Received 26 April 2023; accepted 2 August 2023; published 17 August 2023)

We show that pressure applied to twisted WSe_2 can enhance the many-body gap and region of stability of a fractional Chern insulator at filling $\nu = 1/3$. Our results are based on exact diagonalization of a continuum model, whose pressure dependence is obtained through *ab initio* methods. We interpret our results in terms of a *magic line* in the pressure-vs-twist angle phase diagram: along the magic line, the bandwidth of the topmost moiré valence band is minimized while simultaneously its quantum geometry resembles that of an ideal Chern band. We expect our results to generalize to other twisted transition metal dichalcogenide homobilayers.

DOI: 10.1103/PhysRevResearch.5.L032022

Introduction. Moiré materials provide a highly tunable platform where many quantum phases of matter can be predicted, simulated, and explored. Of particular interest is the potential to realize a fractional Chern insulator (FCI), the zero field analog of the fractional quantum Hall (FQH) effect [1]. FCIs appear in a number of lattice models with fractionally filled flat Chern bands [2–9]. While these early models lacked a clear electronic realization, the unique interplay between topology and interactions in moiré materials brings the experimental realization of FCIs within reach: recently FQH-like states in magic angle twisted bilayer graphene (TBG) have been observed under reasonably small magnetic fields ($B \sim 5$T) [10]. But as the field is reduced, the finite-field ground state becomes unstable to a charge density wave (CDW), consistent with the close competition between the FCI and CDW phases found in theoretical studies [11–16].

Thus, an experimental realization of the long-sought fractional quantum Hall physics at zero field remains to be found. Twisted transition metal dichalcogenides (TMDs) offer a promising alternative platform, as we will now explain. Chern bands were predicted in certain TMD homo- [17] and heterobilayers [18] and experimentally confirmed in $MoTe_2/WSe_2$ [19–21]. Regarding homobilayers, while Chern bands were not observed in twisted WSe_2 in the range 4–5° [22,23], subsequent numerical studies predicted FCI ground states at filling $\nu = 1/3$ of the topmost moiré band at smaller twist angles (∼1.5°) in twisted $MoTe_2$ [24] and WSe_2 [25].

In this work, we show that pressure applied to twisted WSe_2 provides a new tuning knob to enhance the stability of the FCI phase. Specifically, we introduce a region in the pressure-vs-twist angle phase diagram where the FCI indicators [14,26–33]—namely bandwidth, Berry curvature fluctuations, and trace of the quantum metric—are near simultaneously optimized. We then use exact diagonalization to demonstrate an FCI ground state at $\nu = 1/3$ stabilized in the region of near-ideal band geometry, whose many-body gap increases with pressure. We further address the competition between this FCI state and a CDW. Though our calculations are specific to twisted WSe_2, we expect similar features to appear in other twisted TMDs, such as $MoTe_2$, where flat topological bands emerge.

Moiré TMD topological bands under pressure. The low-energy physics of twisted homobilayers such as WSe_2 or $MoTe_2$ can be accurately described by a continuum model. The most general valley-projected Hamiltonian is given, in layer space, by [17,34]

$$\mathcal{H}^K = \begin{pmatrix} h^b(\boldsymbol{k}) & T(\boldsymbol{r}) \\ T^\dagger(\boldsymbol{r}) & h^t(\boldsymbol{k}) - E_{\text{off}} \end{pmatrix}. \tag{1}$$

Due to spin-valley locking, carriers have only one pseudospin degree of freedom. The Hamiltonian describing the other

*na.morales92@utexas.edu
†jennifer.cano@stonybrook.edu

valley is related by time-reversal symmetry. The diagonal terms of Eq. (1) describe carriers populating the topmost valence band of either the bottom (b) or top (t) layer. They consist of the quadratic dispersion of a single TMD layer folded into the moiré Brillouin zone, plus the moiré potential $\Delta^{b/t}(\mathbf{r})$ due to the presence of the other layer, i.e.,

$$h^{b/t}(\boldsymbol{k}) = -\frac{\hbar^2}{2m^*}(\boldsymbol{k} - \boldsymbol{k}_{b/t})^2 + \Delta^{b/t}(\boldsymbol{r}), \tag{2}$$

$$\Delta^{b/t}(\boldsymbol{r}) = 2V_m \sum_{j=1,3,5} \cos(\boldsymbol{b}_j \cdot \boldsymbol{r} \pm \psi), \tag{3}$$

where $\boldsymbol{k}_{b/t} = 4\pi/\sqrt{3}a_M(-1/2, \pm 1/2\sqrt{3})$ are momentum shifts, the vectors $\mathbf{b}_j = 4\pi/\sqrt{3}a_M(\cos(\pi j/3), \sin(\pi j/3))$ belong to the first shell of reciprocal lattice vectors, with a_M the moiré length, m^* is the effective carrier mass, and V_m and ψ are parameters that determine the strength and spatial pattern of the moiré potential, respectively. The interlayer tunneling in Eq. (1) is given by

$$T(\mathbf{r}) = \omega\left(1 + e^{i\frac{2\pi}{3}\alpha}e^{i\mathbf{b}_2\cdot\mathbf{r}} + e^{i\frac{2\pi}{3}2\alpha}e^{i\mathbf{b}_3\cdot\mathbf{r}}\right), \tag{4}$$

where ω is the tunneling amplitude, $\alpha = 0$ for AA stacking (0° rotation between layers, as considered in this paper) and $\alpha = 1$ for AB stacking (180° rotation between layers) [35]. Finally, E_{off} describes the offset between the two topmost bands from each layer, which vanishes for homobilayers in the absence of a displacement field, i.e., an interlayer potential difference. The effect of displacement field has been studied [25,36] and tends to make bands more dispersive, disfavoring FCI stabilization [19,20]; henceforth we set $E_{\text{off}} = 0$.

We focus on twisted AA-stacked WSe_2. Using *ab initio* calculations [37], we obtain an effective mass $m^* = 0.337\, m_0$ and compute the continuum model parameters V_m, ψ, ω over a range of experimentally achievable pressures P or equivalently, sample compression percentages. The behaviors of V_m and ω as a function of sample compression and pressure are shown in Fig. 1(a), while the corresponding evolution of the phase ψ is shown in Fig. 1(b). Both the tunneling amplitude ω and moiré strength V_m increase quadratically with compression percentage, supporting the intuition that applied pressure pushes the layers closer together, increasing both the interlayer tunneling and the moiré potential. A similar trend was predicted in TBG [38], followed by experimental realization [39,40]. Thus, we expect the same tendency to hold for other twisted TMD homobilayers like $MoTe_2$ [37]. Figure 1(c) shows an example of the obtained bandstructure at $P = 2$ GPa. For the parameter range considered in this work, the topmost moiré valence band is always topological with Chern number $C_{K/K'} = \pm 1$, consistent with previous calculations at $P = 0$ [17,35]. Time-reversal symmetry enforces that the Chern numbers at valley K and K' are opposite.

FCI indicators. Comparing a Chern band to the lowest Landau level (LLL) yields single-particle indicators of the stability of a putative FCI phase when the Chern band is partially filled [7,8]. Specifically, the LLL has vanishing bandwidth, homogeneous Berry curvature, and an ideal quantum geometry [9,14,26–28,41–43]. Though the quantum geometry has been an intense subject of recent study, particularly in relation to TBG, it has not been studied in moiré TMDs.

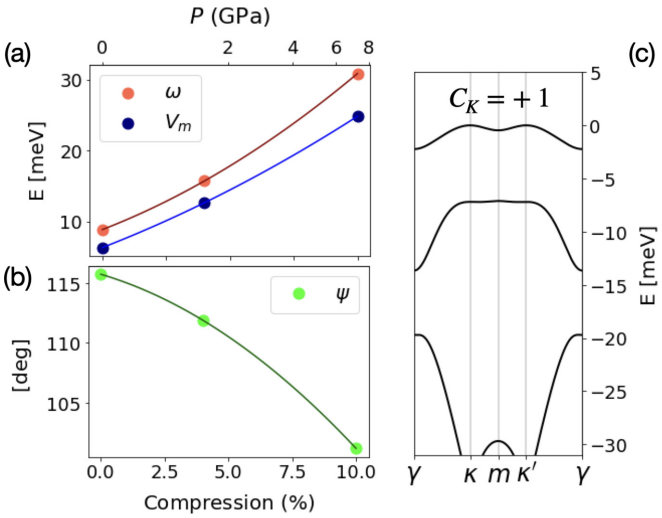

FIG. 1. [(a)-(b)] Evolution of continuum model parameters V_m, ω, and ψ for WSe_2 as a function of compression percentage (bottom axis) and applied pressure (top axis). (c) K-valley-projected bandstructure, corresponding to $P = 2$ GPa and for $\theta = 1.8°$. The topmost moiré valence band from valley $K(K')$ has Chern number $C_K = +1$ ($C_{K'} = -1$).

Figure 2(a) shows the bandwidth of the topmost moiré valence band as a function of twist angle and pressure. At vanishing pressure, the bandwidth is a nonmonotonic function of twist angle, exhibiting a minimum at a "magic angle"

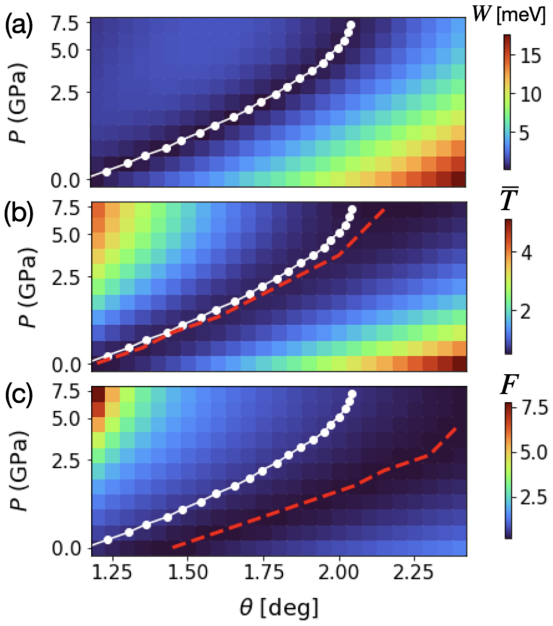

FIG. 2. FCI single-particle indicators of the topmost moiré valence band of WSe_2, plotted as a function of twist angle and pressure: (a) bandwidth W, (b) deviation from the trace condition $\overline{T}$, and (c) Berry curvature fluctuations F. The white line in each plot corresponds to the *magic line* where bandwidth is minimized. Dashed red lines in [(b)-(c)] trace the minimum value of the quantity being plotted. There is a region of the phase diagram where the three indicators are simultaneously close to zero.

[17,35]. Figure 2(a) shows that the minimum extends over the full range of pressures considered, resulting in the appearance of a *magic line*, indicated in white and new to this work.

The stability of the FCI phase will also be impacted by the geometric properties of the Bloch wavefunctions, as contained in the quantum geometric tensor

$$Q^{ab}_{\boldsymbol{k}} = \langle D^a_{\boldsymbol{k}} u_{\boldsymbol{k}} | D^b_{\boldsymbol{k}} u_{\boldsymbol{k}} \rangle = g^{ab}_{\boldsymbol{k}} + \frac{i}{2}\epsilon^{ab}\Omega_{\boldsymbol{k}}, \tag{5}$$

where $D^a_{\boldsymbol{k}} \equiv \partial^a_{\boldsymbol{k}} - iA^a_{\boldsymbol{k}}$ is the covariant derivative, $A^a_{\boldsymbol{k}} = -i\langle u_{\boldsymbol{k}} | \partial^a_{\boldsymbol{k}} u_{\boldsymbol{k}} \rangle$ is the Berry connection and $u_{\boldsymbol{k}}$ is the periodic part of the Bloch function. The right-hand side of Eq. (5) expresses the quantum geometric tensor in terms of the Fubini-Study metric $g^{ab}_{\boldsymbol{k}}$ and the Berry curvature $\Omega_{\boldsymbol{k}}$, which satisfy the inequality $\omega_{\boldsymbol{k},ab}\, g^{ab}_{\boldsymbol{k}} \geqslant |\Omega_{\boldsymbol{k}}|$ [26], for each momentum $\boldsymbol{k}$ and unit-determinant matrix $\omega_{\boldsymbol{k},ab}$. A band for which a $\boldsymbol{k}$–independent matrix ω_{ab} exists that saturates the previous inequality, i.e., $\omega_{ab}\, g^{ab}_{\boldsymbol{k}} = \Omega_{\boldsymbol{k}}$, is said to satisfy the generalized trace condition; a dispersionless band satisfying this condition is called an *ideal flat band* [28]. The Bloch functions of an ideal flat band admit a universal analytical form closely related to the LLL wave functions [28,44–47]. As a consequence, FQH–like ground states are stable under short-ranged interactions in ideal flat bands.

Beyond the LLL, models satisfying the ideal band condition include the chiral model of TBG [14,48–51], Dirac fermions in a nonuniform magnetic field [16], the Kapit-Mueller model [52,53], and periodically strained quadratic band materials [54]. Engineering realistic systems with bands close to the ideal limit [55–58] is a promising direction in the search for FCIs. We now show that moiré TMDs host near-ideal flat bands.

We quantify the deviation of moiré TMD bands from the generalized trace condition by [14,15,26–28,41–43]

$$\overline{T} = \int_{\mathrm{BZ}} \frac{d^2\boldsymbol{k}}{A_{BZ}} \left(\overline{\omega}_{ab}\, g^{ab}_{\boldsymbol{k}} - \Omega_{\boldsymbol{k}}\right), \tag{6}$$

where A_{BZ} is the area of the Brillouin zone and $\overline{\omega}_{ab} = \omega_a\omega^*_b + \omega^*_a\omega_b$ is obtained from the eigenvector ω_a of $\overline{Q}^{ab}$ with the smallest eigenvalue; $\overline{Q}^{ab}$ indicates the Brillouin-zone averaged quantum geometric tensor. The behavior of $\overline{T}$ with pressure and twist angle is shown in Fig. 2(b), which reveals that the line of minimum $\overline{T}$ nearly coincides with the magic line defined by minimum bandwidth.

Finally, the LLL also exhibits $\boldsymbol{k}$-independent Berry curvature. Figure 2(c) shows the Berry curvature fluctuations

$$F = \left[\int_{BZ} \frac{d^2\boldsymbol{k}}{A_{BZ}} \left(\frac{\Omega_{\boldsymbol{k}}}{2\pi} - C\right)^2\right]^{1/2}, \tag{7}$$

where C is the Chern number, as a function of twist angle and pressure. Notably, while the lines of minimum bandwidth and trace deviations almost coincide, the line of minimum Berry curvature fluctuations is distinct. In an ideal band, such as those of chiral TBG, W, $\overline{T}$, and F all vanish simultaneously.

Pressure-twist angle phase diagram. Motivated by the existence of the region in Fig. 2 where W, $\overline{T}$, and F are simultaneously small, we proceed to study many-body ground states in the pressure-vs-twist angle phase space at fractional band filling. Our approach is to write the fully interacting Hamiltonian in momentum space, where the single-particle term comes from the band energies of the continuum model and interactions are projected onto the topmost moiré band. This projection reduces the Hilbert space, allowing for exact diagonalization to obtain the ground state and excited states. Labeling the single-particle energies and eigenstates from the topmost moiré band of Eq. (1) as $\epsilon_{\mathbf{k}}$ and $|u_{\mathbf{k}}\rangle$, respectively, the interacting Hamiltonian reads

$$H = \sum_{\boldsymbol{k}} \epsilon_{\boldsymbol{k}} c^\dagger_{\boldsymbol{k}\sigma} c_{\boldsymbol{k}\sigma} + \frac{1}{2}\sum_{\substack{\boldsymbol{k},\boldsymbol{k}'\boldsymbol{q} \\ \sigma,\sigma'}} V^{\sigma,\sigma'}_{\boldsymbol{k},\boldsymbol{k}',\boldsymbol{q}} c^\dagger_{\boldsymbol{k},\sigma} c^\dagger_{\boldsymbol{k}',\sigma'} c_{\boldsymbol{k}'-\boldsymbol{q},\sigma'} c_{\boldsymbol{k}+\boldsymbol{q},\sigma}. \tag{8}$$

Here σ/σ' are valley indices and $c^\dagger_{\boldsymbol{k},\sigma}$ creates a hole with momentum $\boldsymbol{k}$ in valley σ. The gate-screened Coulomb interaction elements projected to the topmost band are

$$V^{\sigma,\sigma'}_{\boldsymbol{k},\boldsymbol{k}',\mathbf{q}} = \frac{1}{A}\sum_{\boldsymbol{G}} \Lambda^{\mathbf{q}+\boldsymbol{G}}_{\boldsymbol{k},\sigma} \Lambda^{-\mathbf{q}-\boldsymbol{G}}_{\boldsymbol{k}',\sigma'} \frac{2\pi e^2}{\varepsilon\,\tilde{q}} \tanh(\tilde{q}\,d), \tag{9}$$

where $\tilde{q} = |\boldsymbol{q} + \boldsymbol{G}|$ is the momentum transfer, A is the system area, $\Lambda^{\boldsymbol{q}+\boldsymbol{G}}_{\boldsymbol{k},\sigma} = \langle u_{\boldsymbol{k},\sigma} | u_{\boldsymbol{k}+\boldsymbol{q}+\boldsymbol{G},\sigma} \rangle$ are the form factors, ε is the dielectric constant, and d denotes the distance from the sample to metallic gates; to be concrete, we fix $d = 10$ nm. The projection to the topmost band is justified as long as the interaction scale is smaller than the gap to remote bands. To ensure this condition is met, we fix $\varepsilon = 30$, well within the validity of our band projection. In the Supplemental Material [37], we show results for $\varepsilon = 10$, which we expect is closer to the experimental value. While the phase diagram displays the same qualitative features, the single band projection is not as well justified in that case: a more reliable result requires projecting to the top two bands, which we do not consider in this work.

We diagonalize the Hamiltonian in Eq. (8) at band filling factor $\nu = N/N_s = 1/3$, where N is the number of holes and N_s the number of moiré unit cells, for different finite system sizes N_s. The resulting phase diagram as a function of twist angle and pressure is shown in Fig. 3(a). The colored area between the solid black lines indicates the region where Coulomb interactions induce a fully valley-polarized ground state.

Within the valley-polarized regime, the blue region indicates a ground state in the same universality class as the Laughlin state, i.e., an FCI, which extends over approximately half a degree. The FCI is identified by the many-body spectrum in Fig. 3(b), showing a threefold-degenerate ground state with a clear gap to excited states. Upon flux insertion, the three degenerate ground states evolve into each other and remain separated from all excited states [37]. Figure 3 reveals two important insights: First, applied pressure both extends the range of angles over which the FCI phase can be realized and increases the many-body gap. Second, the *magic line* where W and $\overline{T}$ are minimized lies within the FCI region. This highlights the limits of Berry curvature as an FCI indicator [53].

Adjacent to the FCI phase and within the valley-polarized region is a competing CDW ground state, which dominates when bandwidth and trace deviations become large enough. The many-body spectrum of the CDW phase, shown in Fig. 3(c), has a characteristic threefold ground state

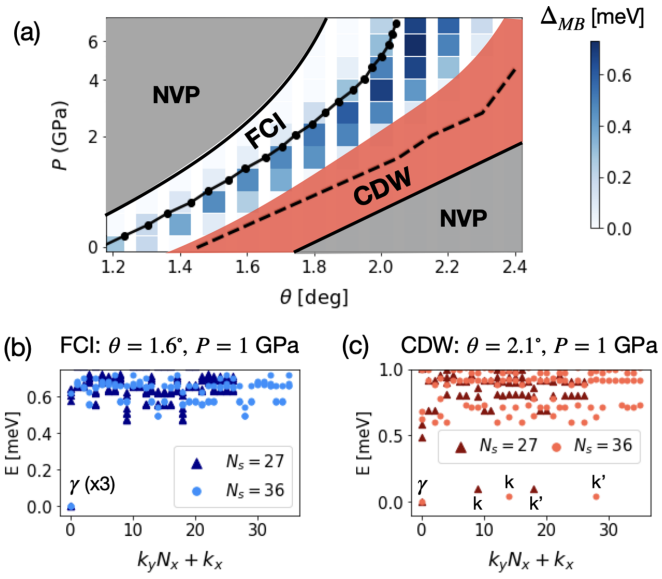

FIG. 3. (a) Phase diagram of twisted bilayer WSe_2 at filling $\nu = 1/3$ as a function of twist angle and pressure. Gray indicates that the ground state is not valley polarized (NVP). Blue and red indicate valley polarization and correspond to an FCI and a CDW, respectively. Blue color scale indicates the many-body gap Δ_{MB} in the FCI phase for $N_s = 27$. The solid line with dots is the magic line and the dashed line indicates the minimum of F. (b) Many-body spectrum for a representative FCI as a function of linearized many-body momentum, displaying a threefold-degenerate ground state at $\boldsymbol{\gamma}$. (c) Many-body spectrum for a CDW state, exhibiting three nearly-degenerate ground states with momenta $\boldsymbol{\gamma}, \boldsymbol{k}, \mathbf{k}'$.

degeneracy consisting of states with many-body momentum $\boldsymbol{\gamma}$, $\mathbf{k}$, and $\mathbf{k}'$.

To further characterize the FCI and CDW phases, Fig. 4 shows the occupation $n(\boldsymbol{q})$, static structure factor $\mathcal{S}(\boldsymbol{q})$, and Berry curvature $\Omega(\boldsymbol{q})$ for representative points within each phase. In the FCI phase, the charge occupation and structure factor are nearly constant, characteristic of a Laughlin-like

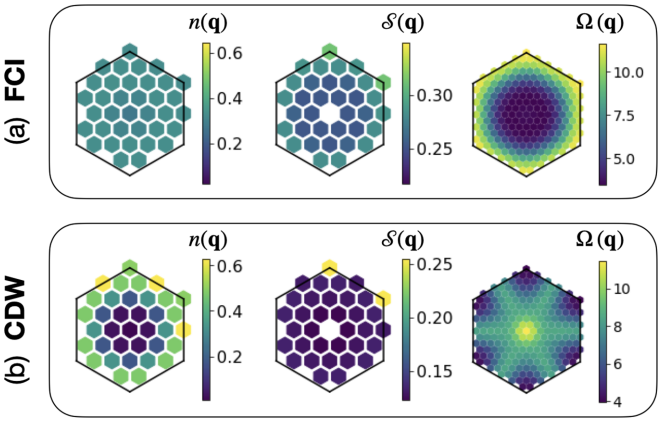

FIG. 4. Ground state occupation $n(\boldsymbol{q})$, static structure factor $\mathcal{S}(\boldsymbol{q})$ and Berry curvature $\Omega(\boldsymbol{q})$ for (a) the FCI ($\theta = 1.6°$, $P = 1$ GPa) and (b) the CDW ($\theta = 2.1°$, $P = 1$ GPa). Results for occupations and structure factors were calculated using $N_s = 36$. The peak in the structure factor at $\boldsymbol{\gamma}$ corresponding to the valley-polarization has been omitted to highlight the structure at other momenta.

state. In contrast, in the CDW phase, the occupation increases towards the edge of the Brillouin zone, while the structure factor shows peaks at the $\mathbf{k}/\mathbf{k}'$ points, indicating moiré translation symmetry breaking to a $\sqrt{3} \times \sqrt{3}$ state. The Berry curvature in the CDW phase is peaked around $\boldsymbol{\gamma}$, where the ground state occupation number vanishes. Thus, the charge carriers do not strongly feel the effective magnetic field, consistent with its trivial topology. In contrast, the ground state occupation in the FCI phase is more uniformly distributed, so that charge carriers feel the Berry curvature throughout the Brillouin zone, resulting in topological order. A similar trend was found in TBG [11,14,59]. However, one difference is that in TBG the Berry curvature is always peaked at $\boldsymbol{\gamma}$, while for TMD homobilayers the peak in Berry curvature moves as the model parameters vary, as seen in Fig. 4.

Discussion. We have proposed semiconductor moiré materials as systems with rich quantum geometry that can be tuned experimentally via applied pressure to stabilize topologically-ordered phases. Specifically, in twisted WSe_2 the "magic angle" where the bandwidth is minimized at zero pressure turns into a *magic line* with similarly small bandwidth at finite pressures. The magic line extends the range of angles over which the FCI phase is stable. Further, the quantum geometry of the band in the region around the magic line is nearly ideal for realizing an FCI.

We provide numerical results that support an FCI ground state, extending previous studies [24,25] to finite pressure. Further, the FCI phase realized at finite pressure has a larger many-body gap than that at zero pressure. Experimentally, we predict that at small twist angles, if an incompressible CDW phase is measured in a moiré TMD homobilayer, applying pressure could drive a transition into an FCI phase. The pressure needed is within experimental reach. Specifically, applied pressures of up to $P \sim 2$ GPa, or equivalently 5% compression, have been realized in TBG [39,40]. In TMDs, pressures up to $P \sim 5$ GPa have been realized at room temperature, and $P \sim 1.4$ GPa [60] at cryogenic temperatures.

As in TBG, the intertwined effects of band dispersion, quantum geometry, and long-range electronic interactions in our model combine to ultimately determine the ground state properties. Despite these complex factors, in TBG the chiral model has provided powerful analytical insight [28,48]. The proximity of our model to the ideal condition motivates a future search for a chiral model of moiré TMDs in a suitable limit. More generally, the question of how perturbations from the ideal limit affect an FCI ground state and its excitations is an open one. The near-ideal Chern band we have described in moiré TMDs suggests that approximating the ground state wavefunctions by modified Landau level wavefunctions is a reasonable approximation [14,28] upon which to build a perturbative study of nonideal Chern bands.

Note added. Soon after our original submission, two independent preprints appeared showing experimental evidence for FCI ground states in twisted $MoTe_2$ [61,62]. Since $MoTe_2$ is described by the same continuum model as WSe_2, i.e., Eq. (1), albeit with different material parameters, we expect that pressure will also stabilize the FCI phase in $MoTe_2$.

Acknowledgments. We thank Valentin Crépel, Allan H. MacDonald, Kin Fai Mak, Andrew J. Millis, and Daniel Parker for insightful discussions. We acknowledge financial

support and computing resources from the Flatiron Institute, a division of Simons Foundation. N.M.D. was supported by the CCQ Pre-Doctoral program. G.R.S. and E.K. acknowledge funding from the Army Research Office under Award No. W911NF-21-2-0147 and from the Simons Foundation Award No. 896626. Z.Z. acknowledges support from a Stanford Science Fellowship. C.R. acknowledges support by the Flatiron Institute IDEA Scholar Program. J.C. acknowledges the Air Force Office of Scientific Research under Grant No. FA9550-20-1-0260 and the Alfred P. Sloan Foundation through a Sloan Research Fellowship. This work was performed in part at Aspen Center for Physics, which is supported by National Science Foundation Grant No. PHY-2210452, and in part at the Kavli Institute for Theoretical Physics, supported by the National Science Foundation under Grant No. NSF PHY-1748958.

[1] D. C. Tsui, H. L. Stormer, and A. C. Gossard, Two-Dimensional Magnetotransport in the Extreme Quantum Limit, Phys. Rev. Lett. **48**, 1559 (1982).

[2] E. Tang, J.-W. Mei, and X.-G. Wen, High-Temperature Fractional Quantum Hall States, Phys. Rev. Lett. **106**, 236802 (2011).

[3] T. Neupert, L. Santos, C. Chamon, and C. Mudry, Fractional Quantum Hall States at Zero Magnetic Field, Phys. Rev. Lett. **106**, 236804 (2011).

[4] K. Sun, Z. Gu, H. Katsura, and S. Das Sarma, Nearly Flatbands with Nontrivial Topology, Phys. Rev. Lett. **106**, 236803 (2011).

[5] D. N. Sheng, Z.-C. Gu, K. Sun, and L. Sheng, Fractional quantum Hall effect in the absence of Landau levels, Nat. Commun. **2**, 389 (2011).

[6] N. Regnault and B. A. Bernevig, Fractional Chern Insulator, Phys. Rev. X **1**, 021014 (2011).

[7] S. A. Parameswaran, R. Roy, and S. L. Sondhi, Fractional quantum Hall physics in topological flat bands, C. R. Phys. **14**, 816 (2013).

[8] E. J. Bergholtz and Z. Liu, Topological flat band models and fractional chern insulators, Int. J. Mod. Phys. B **27**, 1330017 (2013).

[9] Z. Liu and E. J. Bergholtz, Recent developments in fractional Chern insulators, *Reference Module in Materials Science and Materials Engineering* (Elsevier, 2023).

[10] Y. Xie, A. T. Pierce, J. M. Park, D. E. Parker, E. Khalaf, P. Ledwith, Y. Cao, S. H. Lee, S. Chen, P. R. Forrester, K. Watanabe, T. Taniguchi, A. Vishwanath, P. Jarillo-Herrero, and A. Yacoby, Fractional chern insulators in magic-angle twisted bilayer graphene, Nature (London) **600**, 439 (2021).

[11] P. Wilhelm, T. C. Lang, and A. M. Läuchli, Interplay of fractional Chern insulator and charge density wave phases in twisted bilayer graphene, Phys. Rev. B **103**, 125406 (2021).

[12] A. Abouelkomsan, Z. Liu, and E. J. Bergholtz, Particle-Hole Duality, Emergent Fermi Liquids, and Fractional Chern Insulators in Moiré Flatbands, Phys. Rev. Lett. **124**, 106803 (2020).

[13] C. Repellin and T. Senthil, Chern bands of twisted bilayer graphene: Fractional chern insulators and spin phase transition, Phys. Rev. Res. **2**, 023238 (2020).

[14] P. J. Ledwith, G. Tarnopolsky, E. Khalaf, and A. Vishwanath, Fractional Chern insulator states in twisted bilayer graphene: An analytical approach, Phys. Rev. Res. **2**, 023237 (2020).

[15] D. Parker, P. Ledwith, E. Khalaf, T. Soejima, J. Hauschild, Y. Xie, A. Pierce, M. P. Zaletel, A. Yacoby, and A. Vishwanath, Field-tuned and zero-field fractional Chern insulators in magic angle graphene, arXiv:2112.13837.

[16] J. Dong, J. Wang, and L. Fu, Dirac electron under periodic magnetic field: Platform for fractional Chern insulator and generalized Wigner crystal, arXiv:2208.10516.

[17] F. Wu, T. Lovorn, E. Tutuc, I. Martin, and A. H. MacDonald, Topological Insulators in Twisted Transition Metal Dichalcogenide Homobilayers, Phys. Rev. Lett. **122**, 086402 (2019).

[18] Y. Zhang, T. Devakul, and L. Fu, Spin-textured chern bands in ab-stacked transition metal dichalcogenide bilayers, Proc. Natl. Acad. Sci. USA **118**, e2112673118 (2021).

[19] T. Li, S. Jiang, B. Shen, Y. Zhang, L. Li, Z. Tao, T. Devakul, K. Watanabe, T. Taniguchi, L. Fu, J. Shan, and K. F. Mak, Quantum anomalous Hall effect from intertwined moiré bands, Nature (London) **600**, 641 (2021).

[20] W. Zhao, K. Kang, L. Li, C. Tschirhart, E. Redekop, K. Watanabe, T. Taniguchi, A. Young, J. Shan, and K. F. Mak, Realization of the Haldane Chern insulator in a moiré lattice, arXiv:2207.02312.

[21] Z. Tao, B. Shen, S. Jiang, T. Li, L. Li, L. Ma, W. Zhao, J. Hu, K. Pistunova, K. Watanabe, T. Taniguchi, T. F. Heinz, K. F. Mak, and J. Shan, Valley-coherent quantum anomalous Hall state in AB-stacked $MoTe_2/WSe_2$ bilayers, arXiv:2208.07452.

[22] L. Wang, E.-M. Shih, A. Ghiotto, L. Xian, D. A. Rhodes, C. Tan, M. Claassen, D. M. Kennes, Y. Bai, B. Kim, K. Watanabe, T. Taniguchi, X. Zhu, J. Hone, A. Rubio, A. N. Pasupathy, and C. R. Dean, Correlated electronic phases in twisted bilayer transition metal dichalcogenides, Nat. Mater. **19**, 861 (2020).

[23] A. Ghiotto, E.-M. Shih, G. S. S. G. Pereira, D. A. Rhodes, B. Kim, J. Zang, A. J. Millis, K. Watanabe, T. Taniguchi, J. C. Hone, L. Wang, C. R. Dean, and A. N. Pasupathy, Quantum criticality in twisted transition metal dichalcogenides, Nature (London) **597**, 345 (2021).

[24] H. Li, U. Kumar, K. Sun, and S.-Z. Lin, Spontaneous fractional Chern insulators in transition metal dichalcogenide moiré superlattices, Phys. Rev. Res. **3**, L032070 (2021).

[25] V. Crépel and L. Fu, Anomalous Hall metal and fractional Chern insulator in twisted transition metal dichalcogenides, Phys. Rev. B **107**, L201109 (2023).

[26] R. Roy, Band geometry of fractional topological insulators, Phys. Rev. B **90**, 165139 (2014).

[27] S. A. Parameswaran, R. Roy, and S. L. Sondhi, Fractional Chern insulators and the W_∞ algebra, Phys. Rev. B **85**, 241308(R) (2012).

[28] J. Wang, J. Cano, A. J. Millis, Z. Liu, and B. Yang, Exact Landau Level Description of Geometry and Interaction in a Flatband, Phys. Rev. Lett. **127**, 246403 (2021).

[29] M. Claassen, C. H. Lee, R. Thomale, X.-L. Qi, and T. P. Devereaux, Position-Momentum Duality and Fractional Quantum Hall Effect in Chern Insulators, Phys. Rev. Lett. **114**, 236802 (2015).

[30] B. Mera and T. Ozawa, Kähler geometry and Chern insulators: Relations between topology and the quantum metric, Phys. Rev. B **104**, 045104 (2021).

[31] T. Ozawa and B. Mera, Relations between topology and the quantum metric for Chern insulators, Phys. Rev. B **104**, 045103 (2021).

[32] B. Mera and T. Ozawa, Engineering geometrically flat Chern bands with Fubini-Study Kähler structure, Phys. Rev. B **104**, 115160 (2021).

[33] P. J. Ledwith, A. Vishwanath, and D. E. Parker, Vortexability: A unifying criterion for ideal fractional Chern insulators, arXiv:2209.15023.

[34] F. Wu, T. Lovorn, E. Tutuc, and A. H. MacDonald, Hubbard Model Physics in Transition Metal Dichalcogenide Moiré Bands, Phys. Rev. Lett. **121**, 026402 (2018).

[35] T. Devakul, V. Crépel, Y. Zhang, and L. Fu, Magic in twisted transition metal dichalcogenide bilayers, Nat. Commun. **12**, 6730 (2021).

[36] J. Zang, J. Wang, J. Cano, and A. J. Millis, Hartree-fock study of the moiré hubbard model for twisted bilayer transition metal dichalcogenides, Phys. Rev. B **104**, 075150 (2021).

[37] See Supplemental Material at http://link.aps.org/supplemental/10.1103/PhysRevResearch.5.L032022 for: (a) Details on *ab initio* calculations of continuum model parameters as a function of pressure. (b) A discussion on the choosing of parameters ε and d for obtaining the phase diagram. (c) Additional exact diagonalization results, including spectral flow and scaling of many-body gaps in the thermodynamic limit. (d) Details on the different finite geometries used in this study.

[38] S. Carr, S. Fang, P. Jarillo-Herrero, and E. Kaxiras, Pressure dependence of the magic twist angle in graphene superlattices, Phys. Rev. B **98**, 085144 (2018).

[39] M. Yankowitz, S. Chen, H. Polshyn, Y. Zhang, K. Watanabe, T. Taniguchi, D. Graf, A. F. Young, and C. R. Dean, Tuning superconductivity in twisted bilayer graphene, Science **363**, 1059 (2019).

[40] M. Yankowitz, J. Jung, E. Laksono, N. Leconte, B. L. Chittari, K. Watanabe, T. Taniguchi, S. Adam, D. Graf, and C. R. Dean, Dynamic band-structure tuning of graphene moiré superlattices with pressure, Nature (London) **557**, 404 (2018).

[41] T. S. Jackson, G. Möller, and R. Roy, Geometric stability of topological lattice phases, Nat. Commun. **6**, 8629 (2015).

[42] D. Bauer, T. S. Jackson, and R. Roy, Quantum geometry and stability of the fractional quantum hall effect in the hofstadter model, Phys. Rev. B **93**, 235133 (2016).

[43] S. H. Simon and M. S. Rudner, Contrasting lattice geometry dependent versus independent quantities: Ramifications for berry curvature, energy gaps, and dynamics, Phys. Rev. B **102**, 165148 (2020).

[44] J. Wang, S. Klevtsov, and Z. Liu, Origin of Model fractional Chern insulators in all topological ideal flatbands: Explicit color-entangled wavefunction and exact density algebra, arXiv:2210.13487.

[45] J. Dong, P. J. Ledwith, E. Khalaf, J. Y. Lee, and A. Vishwanath, Exact many-body ground states from decomposition of ideal higher Chern bands: Applications to chirally twisted graphene multilayers, Phys. Rev. Res. **5**, 023166 (2023).

[46] B. Mera and T. Ozawa, Uniqueness of Landau levels and their analogs with higher Chern numbers, arXiv:2304.00866.

[47] B. Estienne, N. Regnault, and V. Crépel, Ideal Chern bands are Landau levels in curved space, arXiv:2304.01251.

[48] G. Tarnopolsky, A. J. Kruchkov, and A. Vishwanath, Origin of Magic Angles in Twisted Bilayer Graphene, Phys. Rev. Lett. **122**, 106405 (2019).

[49] J. Wang and Z. Liu, Hierarchy of Ideal Flatbands in Chiral Twisted Multilayer Graphene Models, Phys. Rev. Lett. **128**, 176403 (2022).

[50] P. J. Ledwith, A. Vishwanath, and E. Khalaf, Family of Ideal Chern Flatbands with Arbitrary Chern Number in Chiral Twisted Graphene Multilayers, Phys. Rev. Lett. **128**, 176404 (2022).

[51] J. Wang, Y. Zheng, A. J. Millis, and J. Cano, Chiral approximation to twisted bilayer graphene: Exact intravalley inversion symmetry, nodal structure, and implications for higher magic angles, Phys. Rev. Res. **3**, 023155 (2021).

[52] E. Kapit and E. Mueller, Exact Parent Hamiltonian for the Quantum Hall States in a Lattice, Phys. Rev. Lett. **105**, 215303 (2010).

[53] D. Varjas, A. Abouelkomsan, K. Yang, and E. J. Bergholtz, Topological lattice models with constant Berry curvature, SciPost Phys. **12**, 118 (2022).

[54] X. Wan, S. Sarkar, S.-Z. Lin, and K. Sun, Topological Exact Flat Bands in Two Dimensional Materials Under Periodic Strain, Phys. Rev. Lett. **130**, 216401 (2023).

[55] C. H. Lee, M. Claassen, and R. Thomale, Band structure engineering of ideal fractional Chern insulators, Phys. Rev. B **96**, 165150 (2017).

[56] Q. Gao, J. Dong, P. Ledwith, D. Parker, and E. Khalaf, Untwisting moiré physics: Almost ideal bands and fractional Chern insulators in periodically strained monolayer graphene, arXiv:2211.00658.

[57] X. Wan, S. Sarkar, K. Sun, and S.-Z. Lin, Nearly flat Chern band in periodically strained monolayer and bilayer graphene, arXiv:2302.07199.

[58] S. A. A. Ghorashi, A. Dunbrack, J. Sun, X. Du, and J. Cano, Topological and Stacked Flat Bands in Bilayer Graphene with a Superlattice Potential, Phys. Rev. Lett. **130**, 196201 (2023).

[59] A. Abouelkomsan, K. Yang, and E. J. Bergholtz, Quantum metric induced phases in moiré materials, Phys. Rev. Res. **5**, L012015 (2023).

[60] W. Zhao, E. C. Regan, D. Wang, C. Jin, S. Hsieh, Z. Wang, J. Wang, Z. Wang, K. Yumigeta, M. Blei, K. Watanabe, T. Taniguchi, S. Tongay, N. Y. Yao, and F. Wang, Dynamic tuning of moiré excitons in a WSe_2/WS_2 heterostructure via mechanical deformation, Nano Lett. **21**, 8910 (2021).

[61] J. Cai, E. Anderson, C. Wang, X. Zhang, X. Liu, W. Holtzmann, Y. Zhang, F. Fan, T. Taniguchi, K. Watanabe, Y. Ran, T. Cao, L. Fu, D. Xiao, W. Yao, and X. Xu, Signatures of fractional quantum anomalous Hall states in twisted $MoTe_2$ bilayer, Nature (2023), doi: 10.1038/s41586-023-06289-w.

[62] Y. Zeng, Z. Xia, K. Kang, J. Zhu, P. Knüppel, C. Vaswani, K. Watanabe, T. Taniguchi, K. F. Mak, and J. Shan, Integer and fractional Chern insulators in twisted bilayer $MoTe_2$, arXiv:2305.00973.